Electronic Supplementary Material (ESI) for Soft Matter.

Supplementary Information†: Temperature and Strain Dependent Transient Microstructure and Rheological Responses of Endblock Associated Triblock Gels of Different Block Lengths in a Midblock Selective Solvent

Rosa Maria Badani Prado,[†] Satish Mishra,[†] Humayun Ahmad,[†] Wesley R. Burghardt,[‡] and Santanu Kundu[*,†]

†*Dave C. Swalm School of Chemical Engineering, Mississippi State University, MS State, MS 39762.*

‡*Department of Chemical Engineering, Northwestern University, Evanston, Illinois 60208*

E-mail: santanukundu@che.msstate.edu

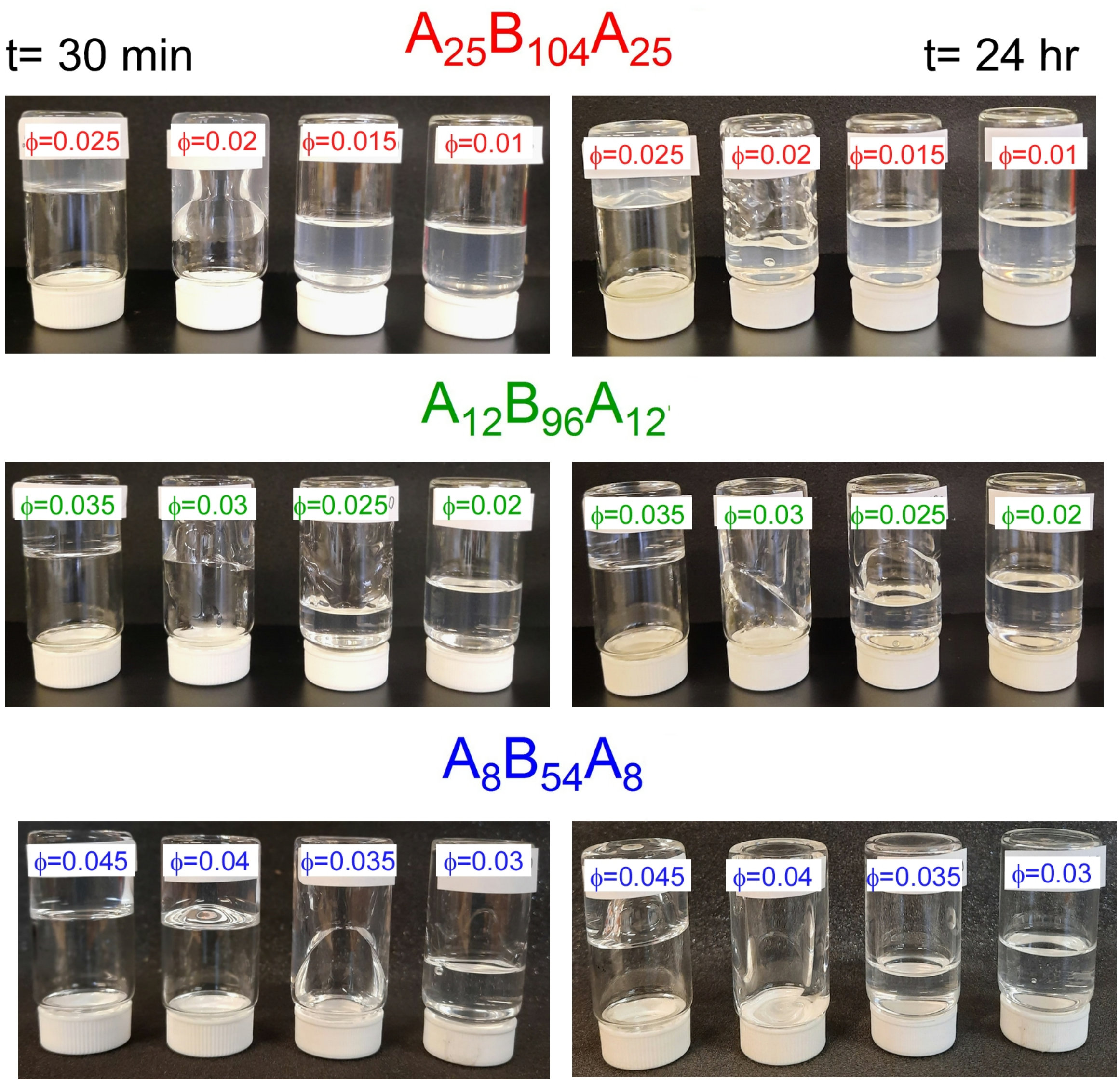

Figure S1: Vial inversion test performed for 30 min and 24 hrs for different ϕ of $A_{25}B_{104}A_{25}$, $A_{12}B_{96}A_{12}$, and $A_8B_{54}A_8$ polymers. The gels were allowed to cool for 5 hrs before inverting the vials. The ϕ at which a gel did not flow in 24 hrs was identified as $\approx \phi^*$.

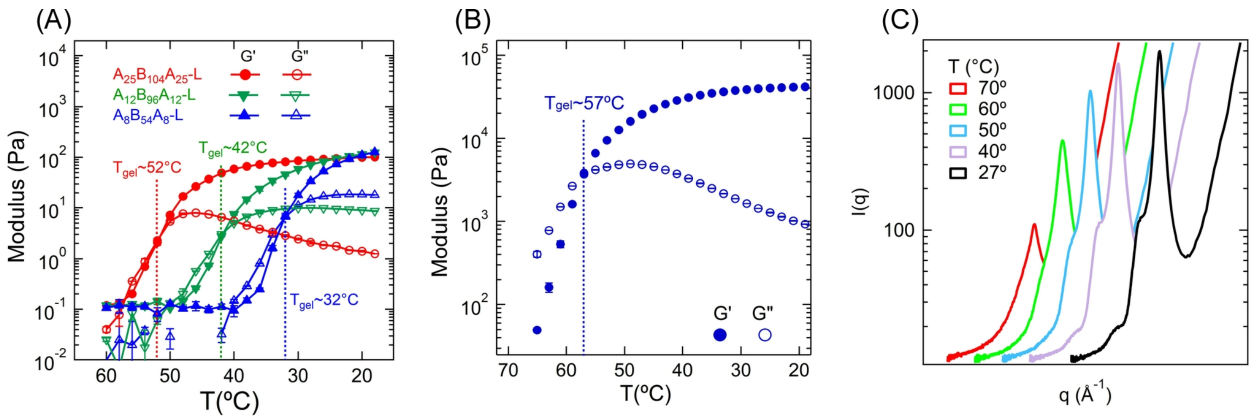

Figure S2: Dynamic moduli G' and G'' obtained from the temperature sweep experiments as a function of temperature (T) for (A) $A_{25}B_{104}A_{25}$-L, $A_{12}B_{96}A_{12}$-L, and $A_8B_{54}A_8$-L, (B) $A_{12}B_{96}A_{12}$-H. (C) $I(q) - q$ plots at T=70, 60, 50, 40, and 27 °C. These figures are similar to as Figure 2A, Figure 8A, and Figure 8B, but here the temperature-axis is presented from high to low.

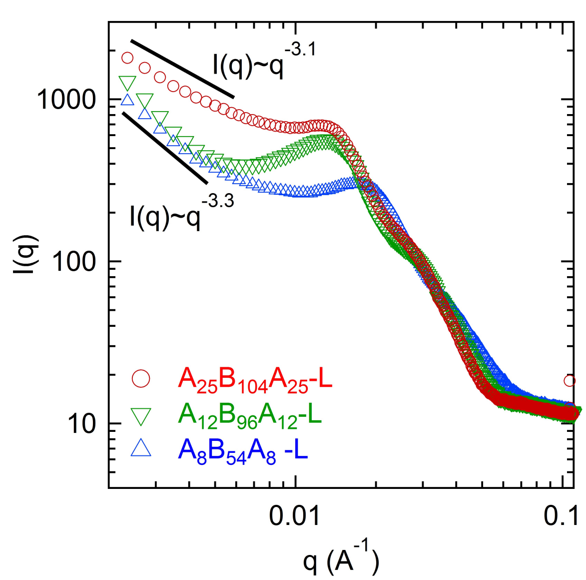

Figure S3: $I(q) - q$ plots for $A_{25}B_{104}A_{25}$-L, $A_{12}B_{96}A_{12}$-L, and $A_8B_{54}A_8$-L for γ_0=0 (without any applied strain).

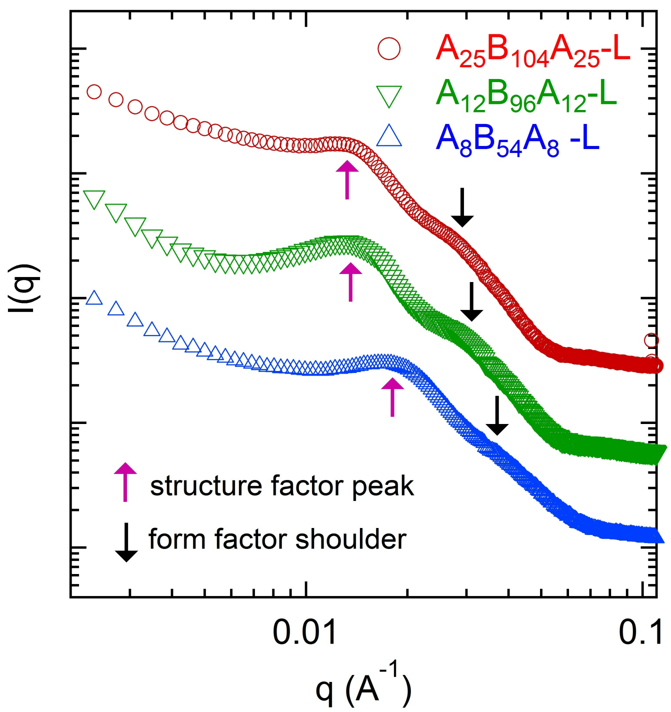

Figure S4: $I(q) - q$ plots for $A_{25}B_{104}A_{25}$-L, $A_{12}B_{96}A_{12}$-L, and $A_8B_{54}A_8$-L . Here $A_{12}B_{96}A_{12}$ and $A_{25}B_{104}A_{25}$-L are shifted along $I(q)$ axis by 5 and 25 times, respectively, of their values.

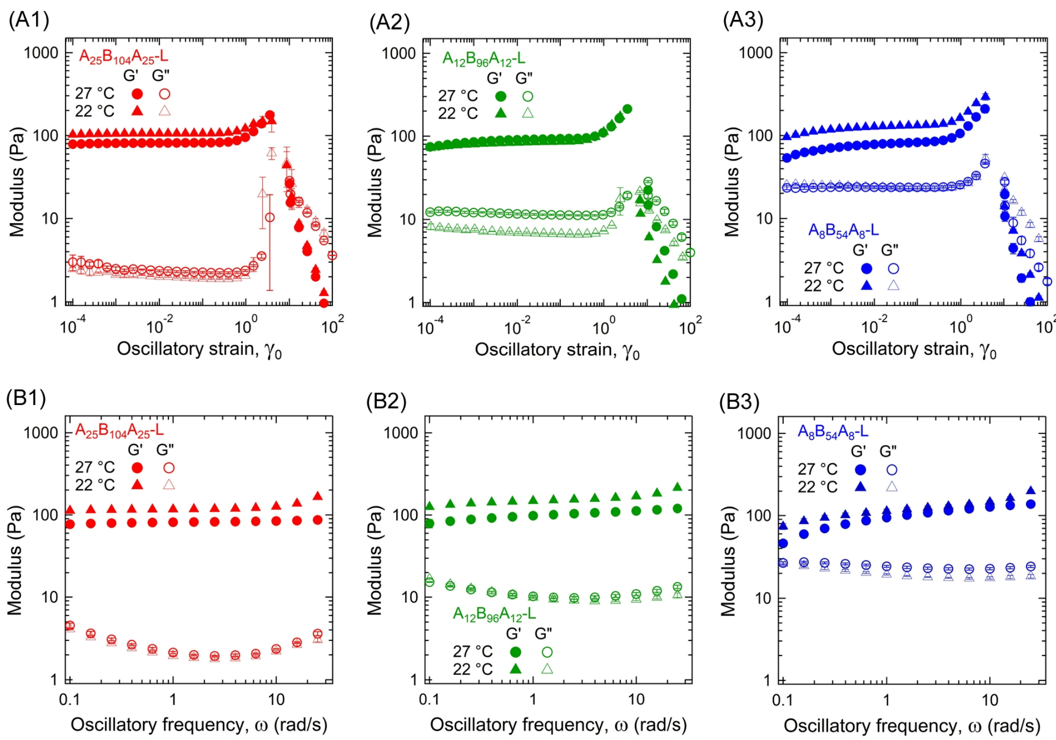

Figure S5: Dynamic moduli G' and G'' obtained from the amplitude sweep experiments for (A1) $A_{25}B_{104}A_{25}$-L, (A2)$A_{12}B_{96}A_{12}$-L, and (A3)$A_8B_{54}A_8$-L for 27 and 22 °C. Dynamic moduli G' and G'' obtained from the frequency sweep experiments for (B1) $A_{25}B_{104}A_{25}$-L, (B2)$A_{12}B_{96}A_{12}$-L, and (B3)$A_8B_{54}A_8$-L for 27 and 22 °C.

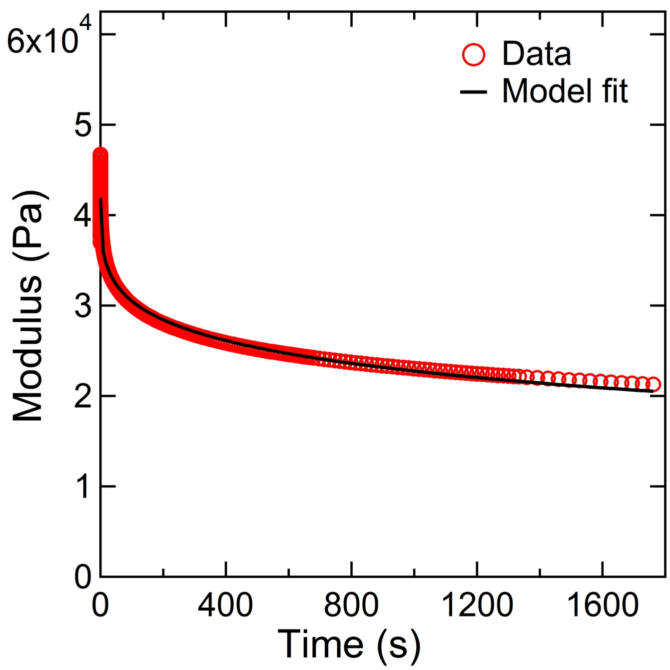

Figure S6: Stress-relaxation data obtained from shear-rheometry for $A_{12}B_{96}A_{12}$-H (high-ϕ). Here, time-dependent shear modulus ($G(t)$) is plotted as a function of time (t). The solid line denotes the model fit with a stretched-exponential model over the range of 0.01 to 1800 s.

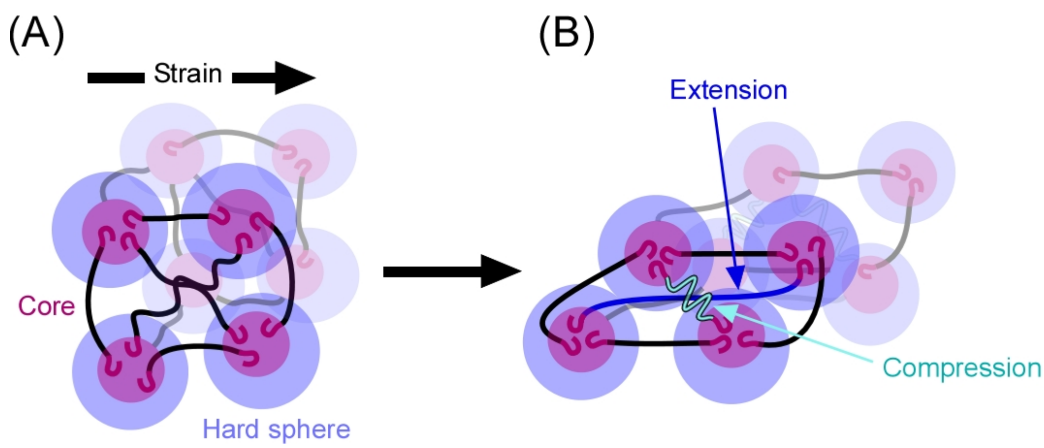

Figure S7: A schematic representation of change in microstructure of gel corresponding to Figure 9C. (A) Microstructure of gel at static condition and (B) Deformed microstructure with chain extension and compression are shown.

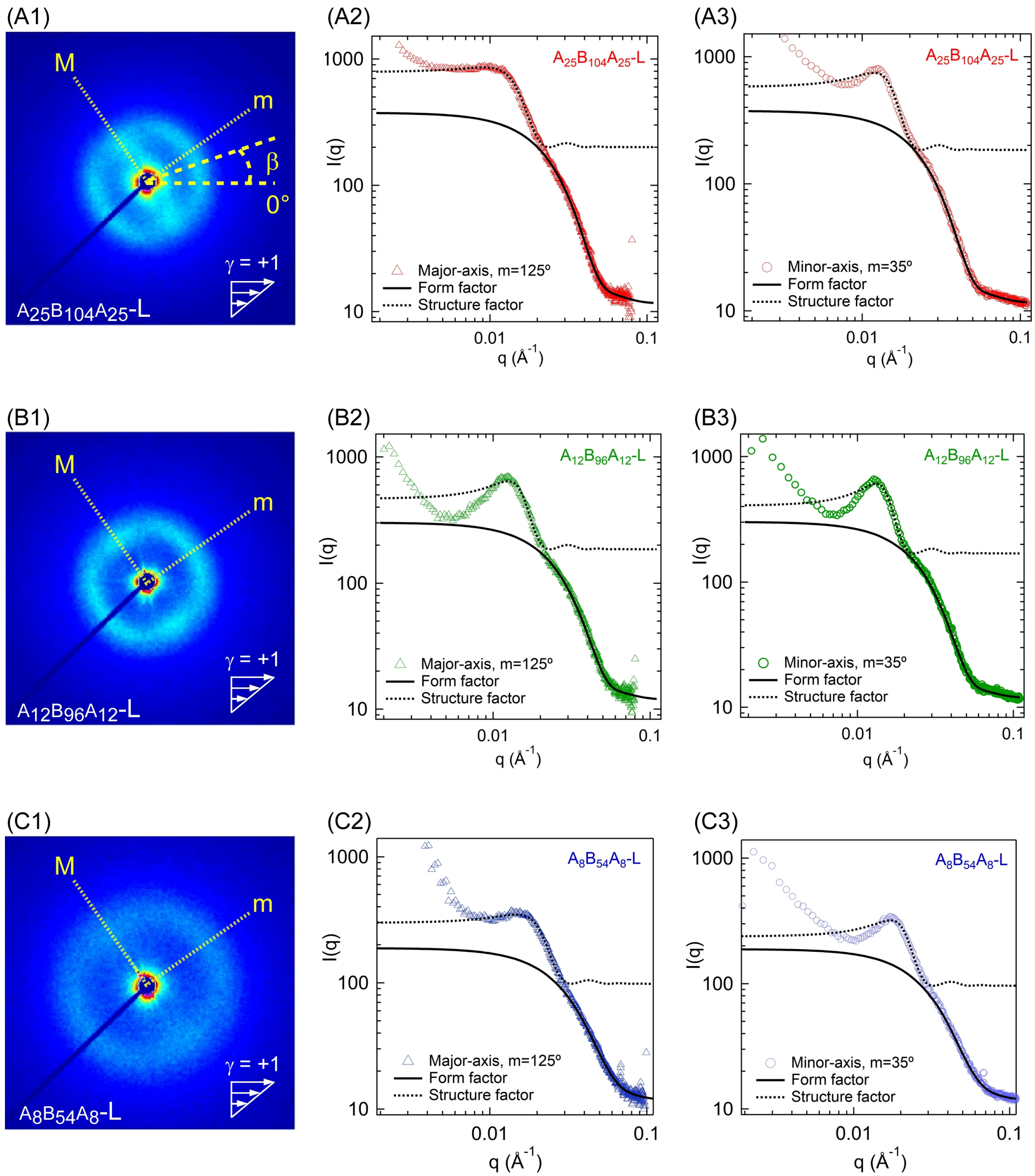

Figure S8: Effect of intracycle strain on $A_{25}B_{104}A_{25}$-L, $A_{12}B_{96}A_{12}$-L, and $A_8B_{54}A_8$-L obtained from RheoSAXS experiments. 2D-scattering patterns at γ=+1 (clockwise) are shown in the left column (A1-3). The corresponding $I(q) - q$ curves along the major-axis (M) (center column, B1-3), and minor-axis (m) (right column C1-3) for (A) $A_{25}B_{104}A_{25}$-L, (B) $A_{12}B_{96}A_{12}$-L, and (C) $A_8B_{54}A_8$-L. The respective lines represent the fit with polydispersed spheres form factor and hard-sphere structure factor models to the experimental data. The representation β-angle is also shown in A1. The fitted parameters are presented in Table 3 in main text.

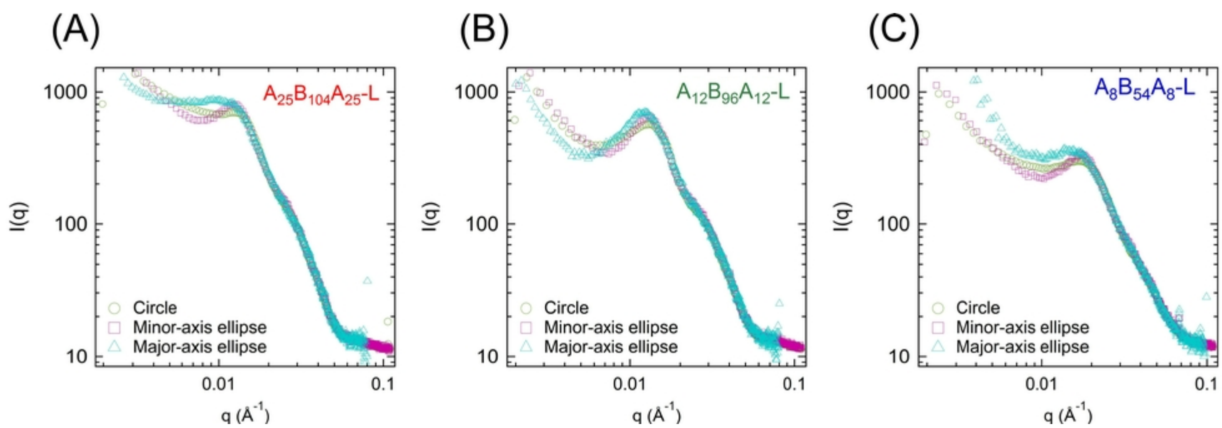

Figure S9: $I(q) - q$ plots of (A)$A_{25}B_{104}A_{25}$-L, (B)$A_{12}B_{96}A_{12}$-L, and (C)$A_8B_{54}A_8$-L obtained by estimating circular average of 2D pattern, along minor-axis, and along major-axis depicting the overlap for $0.01 \leq q \leq 0.08$ Å^{-1}.

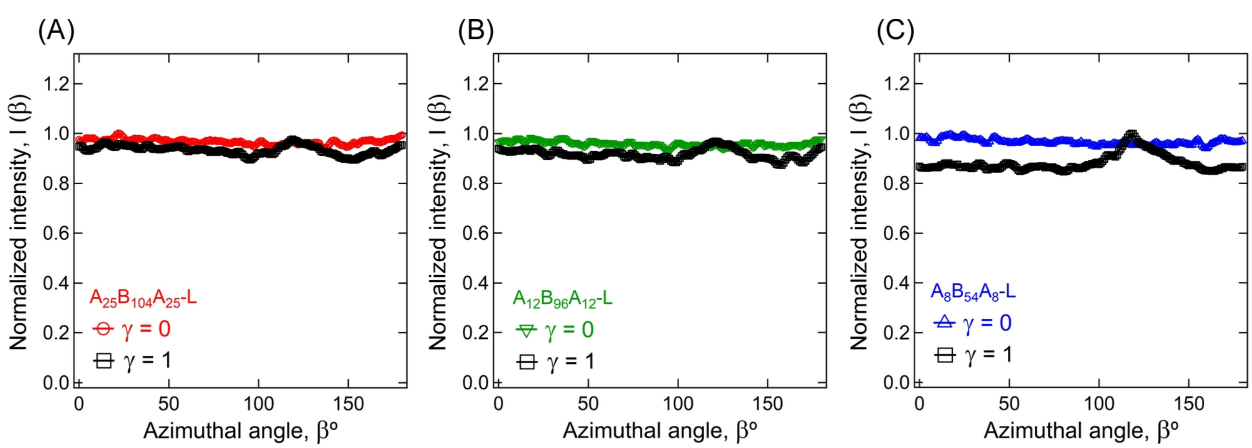

Figure S10: Normalized $I(q) - \beta$ plots for (A)$A_{25}B_{104}A_{25}$-L, (B)$A_{12}B_{96}A_{12}$-L, and (C)$A_8B_{54}A_8$-L for γ=0 and 1 obtained for the q range of 0.01 to 0.05 Å^{-1}.

Table S1: Energy dissipated over a strain cycle (ΔE), Chebyshev elastic coefficients e_1 and e_3, ratio of Chebyshev coefficients (e_3/e_1), and strain-stiffening ratio (S) for different γ_0 values for $A_{25}B_{104}A_{25}$-L, $A_{12}B_{96}A_{12}$-L, and $A_8B_{54}A_8$-L.

		γ_0				
		0.62	0.96	1.47	2.24	3.50
$A_{25}B_{104}A_{25}$-L	ΔE (Pa)	1.28	3.25	8.82	26.42	91.08
	e_1 (Pa)	88.29	96.52	112.57	140.30	185.89
	e_3 (Pa)	1.38	2.89	5.12	7.99	11.87
	e_3/e_1(%)	1.57	3.00	4.55	5.69	6.39
	S	0.06	0.12	0.17	0.22	0.24
$A_{12}B_{96}A_{12}$-L	ΔE (Pa)	6.65	16.34	41.15	111.60	358.42
	e_1 (Pa)	99.10	109.47	129.03	161.11	210.39
	e_3 (Pa)	1.67	3.22	5.22	7.55	11.51
	e_3/e_1(%)	1.68	2.94	4.05	4.69	5.47
	S	0.07	0.11	0.16	0.18	0.21
$A_8B_{54}A_8$-L	ΔE (Pa)	14.20	35.61	91.67	253.76	984.50
	e_1 (Pa)	90.67	102.86	125.61	162.33	192.10
	e_3 (Pa)	1.40	2.71	4.34	6.14	7.66
	e_3/e_1(%)	1.54	2.64	3.46	3.78	3.99
	S	0.06	0.10	0.13	0.15	0.15

Table S2: Information related to the microstructure of low-ϕ gels. Here, M is triblock copolymer molecular weight, ϕ is volume fraction, ρ is polymer density, D is inter-aggregate distance, r_c is core radius, and $R_{\theta,e-e}$ is end-to-end distance of B-blocks considering θ-solvent. Here, Kuhn length of B-block as 1.71 nm and Kuhn molecular weight of 0.844 kg/mol were considered for calculations.

Gel	M (kg/mol)	ϕ	ρ (kg/m^3)	D (nm)	$D-2r_c$ (nm)	$R_{\theta,e-e}$ (nm)	Stretch ratio
$A_{25}B_{104}A_{25}$-L	154	0.03	1080	49.7	36.0	18.9	1.9
$A_{12}B_{96}A_{12}$-L	120	0.04	1080	46.9	34.0	18.1	1.9
$A_8B_{54}A_8$-L	70	0.05	1080	35.5	27.6	13.6	2.0